



HAL
open science

Self-organization of surfaces on the nanoscale by topography-mediated selection of quasi-cylindrical and plasmonic waves

Anton Rudenko, Cyril Mauchair, Florence Garrelie, Razvan Stoian,
Jean-Philippe Colombier

► To cite this version:

Anton Rudenko, Cyril Mauchair, Florence Garrelie, Razvan Stoian, Jean-Philippe Colombier. Self-organization of surfaces on the nanoscale by topography-mediated selection of quasi-cylindrical and plasmonic waves. *Nanophotonics*, 2019, 10.1515/nanoph-2018-0206 . ujm-02003580

HAL Id: ujm-02003580

<https://ujm.hal.science/ujm-02003580>

Submitted on 1 Feb 2019

HAL is a multi-disciplinary open access archive for the deposit and dissemination of scientific research documents, whether they are published or not. The documents may come from teaching and research institutions in France or abroad, or from public or private research centers.

L'archive ouverte pluridisciplinaire **HAL**, est destinée au dépôt et à la diffusion de documents scientifiques de niveau recherche, publiés ou non, émanant des établissements d'enseignement et de recherche français ou étrangers, des laboratoires publics ou privés.

Research article

Anton Rudenko*, Cyril Maucclair, Florence Garrelie, Razvan Stoian
and Jean-Philippe Colombier*

Self-organization of surfaces on the nanoscale by topography-mediated selection of quasi-cylindrical and plasmonic waves

<https://doi.org/10.1515/nanoph-2018-0206>

Received November 27, 2018; revised January 9, 2019; accepted January 12, 2019

Abstract: Using coupled electromagnetic and hydrodynamic calculations, we elucidate theoretically the topographic transition from a random metallic surface to a periodic sub-wavelength grating by ultrashort laser ablation. The origin of this transition lies in the successive selection of hybrid surface waves scattered by random nanoholes. Contrary to the common belief that surface plasmon polaritons play the dominant role in the process and define the grating periodicity, we show that both quasi-cylindrical and surface plasmon waves are involved, whereas the diversity in the resulting spacings $\lambda/2-\lambda$ (λ is the laser wavelength) is the manifestation of a broad frequency overlap of these waves, controlled by their relative phase shifts with respect to the plasmonic counterparts. The topography evolution imposes the dominant contribution to the surface sub-wavelength pattern by selecting the appropriate wave character from plasmonic modes to evanescent cylindrical waves. With the radiation dose, the grating periodicity exhibits a pronounced blue shift due to reinforced dipole-dipole coupling between the nanoholes and surface curvatures in the laser-processed area. This allows the creation of regular patterns with tunable periodicity.

Keywords: nanoplasmonics; ultrafast optics; self-organization; laser material processing; surface waves; ripples.

*Corresponding authors: Anton Rudenko and Jean-Philippe Colombier, University of Lyon, UJM-St-Etienne, CNRS, Institute of Optics Graduate School, Laboratoire Hubert Curien UMR 5516, F-42023 Saint-Etienne, France, e-mail: anton.rudenko@univ-st-etienne.fr (A. Rudenko); jean.philippe.colombier@univ-st-etienne.fr (J.-P. Colombier).
<https://orcid.org/0000-0002-8915-8319> (A. Rudenko)

Cyril Maucclair, Florence Garrelie and Razvan Stoian: University of Lyon, UJM-St-Etienne, CNRS, Institute of Optics Graduate School, Laboratoire Hubert Curien UMR 5516, F-42023 Saint-Etienne, France

1 Introduction

The interaction of light with nanostructures on metal surfaces is at the origin of a large variety of amazing phenomena including extraordinary optical transmission through hole arrays [1–4], abnormal optical absorption and Wood's anomalies by diffraction gratings and grooves [5–7], enhanced resonant coupling between nanoholes and nanoparticles [8–11], Anderson localization of light [12, 13], and the self-organization of matter by multipulse laser irradiation [14–17]. In spite of the striking differences between the physical concepts, scenarios based on surface plasmon polariton (SPP) excitation were proposed to explain each of the above phenomena. The frameworks were followed by debates on whether SPPs play the defining role. These discussions were mainly due to the fact that SPP is not the unique surface wave generated by the interaction of light with a single indentation on the metal-dielectric interface [2–4, 18]. Additionally, the efficient excitation of SPP, in contrast to low-efficient light-to-SPP coupling with broad SPP resonances and a strong presence of the reflected light provided by random roughness, requires specific conditions for surface relief, such as the presence of infinite nanoslits, periodic gratings, or arrays of holes [6, 19]. Recently, it was demonstrated that the total scattered field from a single metallic nanoslit consists of the SPP, an evanescent cylindrical wave (CW), and a Norton wave [20, 21]. The dominant contribution is defined by metal/dielectric properties, laser wavelength, and distance from the object. CWs were shown to play a significant role in the extraordinary optical transmission through periodic and random nanohole arrays and to contribute to the interaction of light with all-nanostructured metallic surfaces [3, 4, 22, 23]. Finally, an analytical asymptotic solution for total field scattered by a single sub-wavelength hole was derived [18], making it possible to separate the contributions from the different waves.

Even though the formation of laser-induced periodic surface structure (LIPSS) as a common phenomenon on dielectric, semiconductor, and metal surfaces has already paved the way to high-impact applications in optical data storage, computer holography, security marking, and tribology, their fundamental origin is still debated [14–17, 24–27]. The possibility of SPP excitation on metal–dielectric interfaces with sub-wavelength indentations or depressions [6], commonly present as the counterparts of pristine [24, 28] or laser-induced roughness [17], has persuaded a large part of the research community to accept the dominant role of this phenomenon in ripple formation [14, 15, 26, 29–31]. Sipe et al. derived the scattered field asymptotics at infinite distance from a confined region of surface nanoroughness, including both SPP and radiation remnants with characteristic decays of CW [24, 32], and further confirmed by solution of Maxwell equations; however, the intimate nature of the waves and their interplay have not been uncovered [17, 27, 28, 33]. Along with open debates regarding the nature of the involved surface waves, the origin of low-spatial-frequency LIPSS (LSFL) periods, reported to be significantly smaller than the laser wavelength and the SPP wavelength in the range of $\lambda/2$ – λ and decreasing with the number of applied pulses [25, 31, 34], still remains unclear [14, 28, 30, 31, 34].

In this article, we show that the electromagnetic origin of LIPSS with periodicity $\lambda/2$ – λ is a process of multipulse selection of hybrid standing waves produced by the interference of the incident light with surface wave scattered by nanoholes with comparable contributions of SPP and CW. Two main factors drive the period reduction: enhanced dipole–dipole coupling between nanoholes, and surface curvature at the edges of the ablation crater, dictating the saturation value of well-organized LIPSS. Multipulse numerical simulations based on Maxwell equations, coupled with the two-temperature model and ablation removal criterion, support the proposed scenario and reveal the transition from a rough surface to a pronounced sinusoidal periodic grating.

2 Results and discussion

The geometry of the discussed problem is illustrated in Figure 1. Before analyzing the origin of the complex interference patterns on the metal surface with random sub-wavelength holes, we focus on the individual response of a single hemispherical nanohole at the metal–air interface in Figure 2A–C. The intensity distribution near such a nanohole just below the surface is calculated by the finite-difference time-domain (FDTD) method [35]. Figure 2B

shows that the intensity is enhanced at the interface of the nanohole (we refer to it as a near-field enhancement) but also at discrete periodic positions along the polarization direction at certain distances from the indentation (far field). The closest far-field maximum is the broadest at the distance of $\approx 3\lambda/4$ from the emission center. Further maxima become narrower and are separated by $\approx \lambda$. This feature does not change significantly even if we modify the size, shape, or depth of the nanohole. The intensity distribution here is the product of the interference between the incident light and the scattered light from the surface of the nanohole: $I \approx 2E_{\text{sca}} E_{\text{inc}}$, as the term E_{sca}^2 is negligible. Therefore, the investigation of the interference patterns reduces to the analysis of the scattered fields. To understand the nature of the electric field maxima, we use the analytical asymptotic solution of the electromagnetic scattering by a sub-wavelength hole [18]. The solution allows us not only to define the positions of the maxima, which are in a good agreement with the results of FDTD, but also to separate the contributions of SPP and CW. Figure 2A shows that the maxima of the total scattered field are due to the overlap of phase-shifted waves having comparable contributions. The cylindrical evanescent wave is proportional to $\exp(ik_0 x)/x$ in the vicinity of the nanohole and has a phase shift of $\exp(-i\pi/4)$ with respect to SPP decaying as $\exp[-\text{Im}(k_{\text{sp}})x]/x^{1/2}$, where $k_{\text{sp}} = k_0 \sqrt{\epsilon_m / (1 + \epsilon_m)}$, ϵ_m is the complex permittivity of the metal, and $k_0 = 2\pi/\lambda$ is the

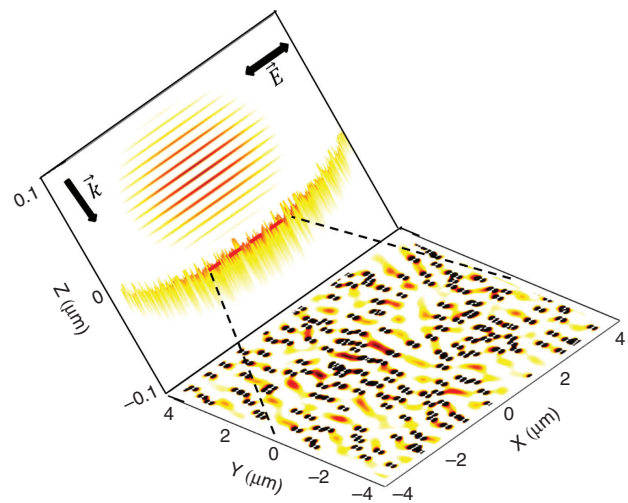


Figure 1: Geometry of the considered problem.

Ultrashort laser light polarized along the X-direction falls on the metal surface with pristine or laser-induced roughness. The transverse plane XY beneath the surface shows the energy deposition including polarization-dependent near and far fields scattered by randomly distributed nanoholes. Here and further, the laser wavelength is fixed as $\lambda = 800$ nm.

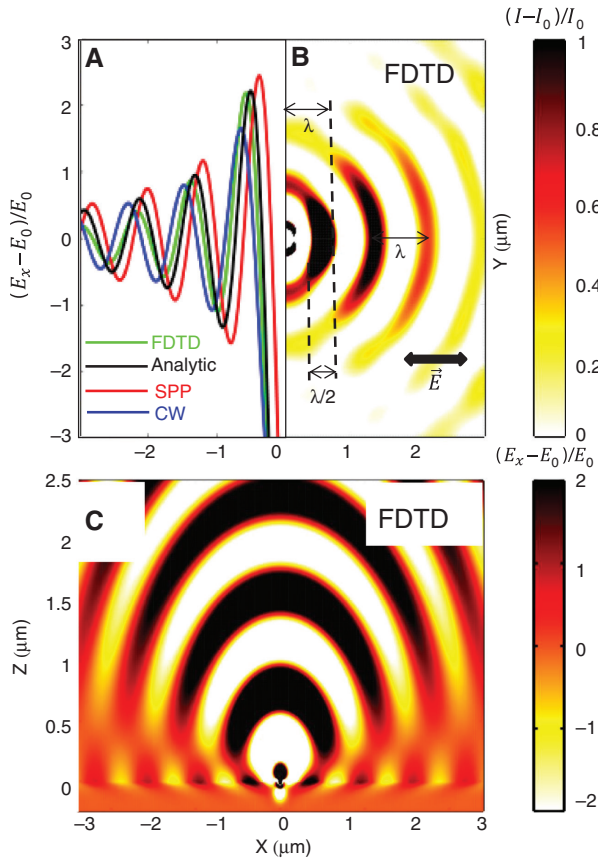


Figure 2: Electromagnetic response of a single hemispherical nanohole on a metal surface. (A) Comparison between FDTD (green) and analytical (black) solution for a single subwavelength hole along the X -direction ($y=0, z=0$). The scattered field E_x is decomposed on the surface plasmon wave (SPP, red) and the quasi-cylindrical wave (CW, blue) contributions. (B) The intensity distribution near a hemispherical nanohole with $R=50$ nm in the transverse plane of a stainless steel surface. (C) The electric field E_x in the propagation plane calculated by FDTD.

wave vector [18, 20]. The phase shift is due to the nature of CWs driven by charge accumulation at the hole edges [36] (see Supplementary Information). Figure 2C shows that SPP, which is confined to the metal–air interface, and CW, decaying more slowly in air and as well as existing at the interface, are mismatched, whereas closest to the nanohole, the extrema of scattered fields are due to the overlap of these waves. For realistic permittivity values and most metals in the optical frequency range, such an overlap inevitably occurs in the vicinity of any nano-object. If the plamonic wave decays even faster than the evanescent CW, as in case of lossy metals, the interference patterns will be mainly due to the CW with linear dispersion relation and will have laser wavelength periodicity.

To elucidate the role of the collective effects of random holes at the metal–air interface, we perform

FDTD simulations with different nanohole concentrations and analyze the results by taking Fourier transforms in Figure 3A, B. In case of hole separation of the same order of or larger than the wavelength, each nanohole acts as an individual source scattering hybrid waves with characteristic intensity maxima close to λ . At smaller separations, the decisive role of the first intensity maximum at $\approx 3\lambda/4$ is seen, which is an indicator of the significant contribution of the evanescent CW [4]. Furthermore, the dominant periodicity shifts toward smaller values in Figure 3B, and the Fourier spectrum becomes more dispersed as the concentration increases. To understand this, we use a semianalytical model based on the coupled-dipole approximation [8] (see Supplementary Information).

The results are first represented in terms of the retarded dipole sum S as a function of the average dipole spacing d , indicating the possibilities of blue shift [$\text{Re}(S) < 0$] or red shift [$\text{Re}(S) > 0$] of the resonant wavelength, as well as broadening [$\text{Im}(S) > 0$] or narrowing [$\text{Im}(S) < 0$] of the spectrum in Figure 3D. The resonant wavelength shifts from the individual nanohole response are then quantitatively estimated (see Supplementary Information) and given as the ordinates of the graph. In fact, the resonant wavelength decreases with decreasing average nanohole spacing in the range $400 \text{ nm} < d < 800 \text{ nm}$. Below 400 nm, the spectrum becomes broader, and only near-field short-range dipole coupling is involved [10]. In this regime, light cannot propagate through the densely packed array of holes because of significant retardation of the surface wave, canceling the interference effects. Above 800 nm, the holes behave as individual, noninteracting emission centers. Finally, $d \approx 625 \text{ nm}$ corresponds to the equilibrium average distance in the narrow spectrum, where no shift is expected. This way, the interhole spacings may decrease from $\approx \lambda$ driven by dipole–dipole coupling of neighboring holes only down to the saturation value $d \approx 3\lambda/4$.

To investigate the evolution of surface relief under realistic multipulse ablation conditions, we perform numerical simulations, where the energy absorption is calculated by Maxwell equations, then the electron–ion heat transfer by the two-temperature model, and the material is removed if the temperature exceeds the boiling point. The procedure is repeated for each new pulse, and therefore the simulations take into account the electromagnetic feedback, i.e., change in the energy deposition due to surface relief modification. The details of the model can be found in Supplementary Information. We show the energy deposition after N pulses on a stainless steel surface with pristine roughness in Figure 4C. The choice of the initial surface conditions at the nanoscale does not influence the final LSFL periodicity, but it may affect the

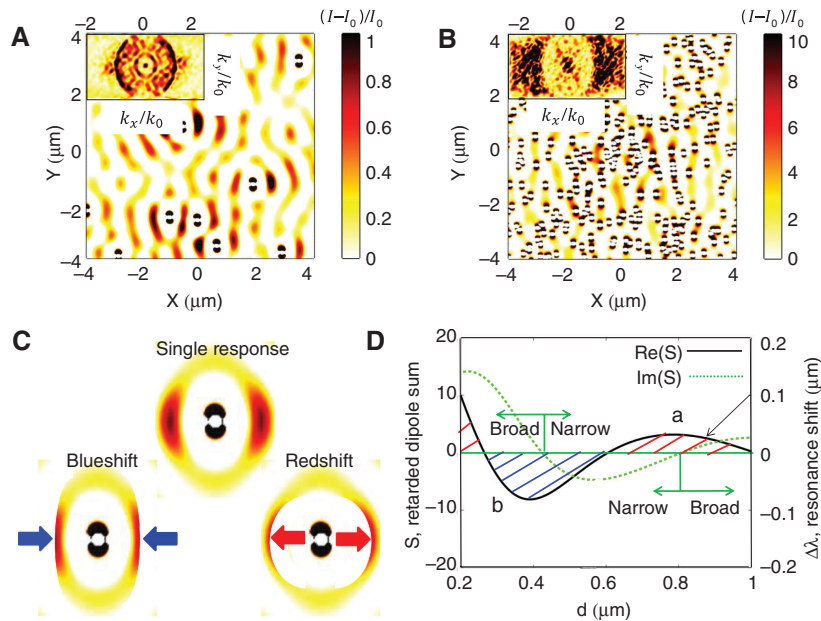


Figure 3: Collective response of randomly distributed nanoholes on a metal surface.

Intensity distribution and the corresponding Fourier transforms on the top-left side of the figure. Nanoholes are of $R=50$ nm and average spacings (A) $d=800$ nm and (B) $d=300$ nm. The wave vectors are normalized to $k_0=2\pi/\lambda$. (C, D) Resonant wavelength shift predictions as a function of d using dipole–dipole interaction semianalytical approach and the concept of the retarded dipole sum S .

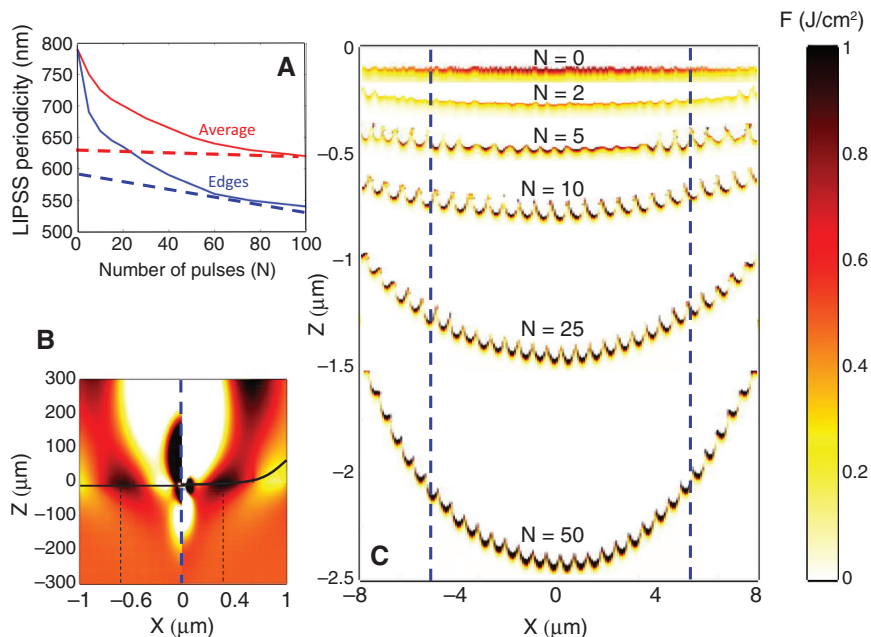


Figure 4: Evolution of surface relief under multipulse irradiation.

(A) Ripple periodicity averaged along all interface (red solid line) and at the edges of the crater (blue solid line) as a function of the number of pulses. The dashed lines indicate the period saturation values. (B) Electric field distributions on a plane metal–air surface (left) and on a curved interface (right). The scale is the same as in Figure 2C. (C) Absorbed energy distribution after irradiation of N pulses of a stainless steel surface with pristine roughness (holes of radius $R=10$ nm and average spacings $d=100$ nm). The laser fluence is 0.5 J/cm^2 .

speed of periodic structure regularization. In our case, the choice of random nanoholes of $R=10$ nm is justified by experimental observations of nanoholes and sub-surface

nanovoid formation after irradiation with the first pulse as a primary step of surface damage, as supported by molecular dynamics simulations [17, 37]. The calculations

have been performed for different fluences, beam waists, and pristine roughness values, in each case resulting in a quasi-periodic ripple formation after 5–10 pulses. Figure 4A shows the multipulse dynamics of the averaged ripple periods from ≈ 750 nm up to saturation at the value ≈ 625 nm after 50–100 pulses. The first value close to the laser wavelength and SPP wavelength is the typical spacing between the interference maxima of an individual nanohole illustrated in Figure 2. The saturation value corresponds to the distance between the closest interference maxima and the nanohole in Figure 2, as well as to the equilibrium average distance between the coupled nanoholes, where no further shift of the resonant wavelength is expected in Figure 3D. Smaller values down to ≈ 500 nm are obtained at the edges of the ablation crater (blue line in Figure 4A), which is the consequence of the surface curvature. In fact, the surface wave has larger phase retardation on the concave interface compared to the plane interface, resulting in the interference maxima shifting closer to the emission center in Figure 4B. This effect is at the origin of the lower saturation values of ripple periodicity after projection on to the plane interface.

The energy is deposited mainly at the bottom of ripples; therefore, the speed of ripple period saturation in ablation by lower fluences is impacted by the initial roughness and exact position of the nanoholes. The higher the fluence, the less sensitive the ablation

removal to nanohole coupling. The simulations indicate that at higher fluences the ablation takes place all along the surface (at the bottoms and at the tips), favoring the role of long-distance interference maxima as in the case of Figure 3A, and the final established periodicity is close to the SPP wavelength. This explains the increase of LIPSS periodicity with increasing laser fluence [31, 38].

Previously, LIPSS periods smaller than λ on metal surfaces have been attributed to grating-assisted or roughness-assisted SPP–laser coupling [14, 30, 31], to transient optical properties of metals due to ultrafast excitation [15, 28], or to changes in local angle of incidence at the edges of ablation craters [28].

The first two scenarios suggest the strong correlation of SPP wavelength with the depth of LIPSS, modeled as a perfect diffraction grating [14, 30, 31]. Efficient coupling between the normally incident light and the diffraction grating requires that the grating period is equal to the effective SPP wavelength for the given surface relief, which is a condition that is never realistically satisfied. Our simulations indicate that the ripple deepening at 5–10 pulses does not result in any significant period decrease, whereas the reduction takes place at a larger number of pulses, conserving almost the same ripple depth in Figure 5A. Furthermore, the multipulse dynamics is unique for each nanostructure having equal depth, invalidating the presence of one global SPP wavelength

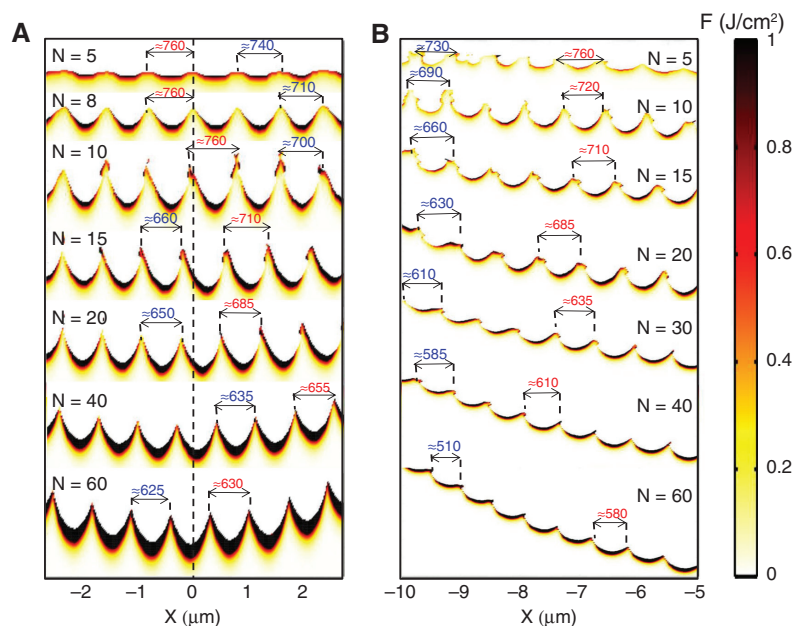


Figure 5: Evolution of ripple periods under multipulse irradiation.

Absorbed energy distribution after irradiation of N pulses (A) at the center and (B) at the edges of the ablation crater. The maximum and minimum spacings between consecutive ridges are marked in nanometers by red and blue, respectively. The irradiation conditions are as in Figure 4.

controlling the dynamics, and depends on the distance between neighboring holes.

The transient changes of optical properties as a function of the electron temperature have been deduced by ab initio calculations [39]. The results reveal the possibility of transition from non-plasmonic to plasmonic behavior for tungsten and significant changes in optical properties of several metals under ultrafast laser irradiation conditions [39]. Our simulations show a pronounced contribution of SPP in scattering from a single nanohole on the surface of excited metals and semiconductors (see Supplementary Information). However, neither the transition to plasmonic state nor the changes in SPP wavelength explain the significant ripple period reduction by multipulse irradiation.

Regarding the change in the local angle of incidence, we propose to relate the period reduction at the edges of the crater to the different speed of surface wave propagation on a curved surface rather than to the effects of geometrical optics or to the fact that the ripple spacings are projected on a plane surface. The simulations show a significant reduction even in case of small ratios of depth ≈ 500 nm to the crater width ≈ 10 μm as in the case of $N=25$ in Figure 4. Figure 5B shows the increasing contrast between the ripple periodicity closer to the center and at the edge, where the curvature is stronger.

The numerical results based on multipulse coupled electromagnetic and hydrodynamic simulations are shown here only for stainless steel. However, the proposed mechanism of periodic surface structure formation is unique for any solids acquiring metallic properties and for any pristine nanometric roughness, resulting in LIPSS formation by laser ablation and regularization of their periods by consecutive irradiation. The material properties may play a role, but establishing laser-induced roughness via hydrodynamic processes is beyond the present model and discussed elsewhere [40].

3 Conclusion

In this article, we showed the involvement of a new class of surface waves (CWs) in the self-organization of LIPSS on metal surfaces with pristine roughness consisting of random nanoholes. We found that sub-wavelength holes on the substrate exhibit a pronounced broad-frequency field enhancement at distances $\lambda/2$ – λ independent of their depth, nanometer size, or shape. To elucidate the complex nature of this pattern, we used the analytical solution for scattered field from an isolated dipole. The analytical results, which showed good agreement with full-vector

Maxwell numerical solution, indicated that the broad-frequency hybrid mode is due to an overlap of phase-shifted evanescent CW and SPP having comparable amplitudes on sub-wavelength distances from the hole.

The collective response of randomly distributed nanoholes was further studied by FDTD simulations and analyzed by a semianalytical dipole–dipole interaction model. Both methods indicate a pronounced blue shift of the spectrum toward lower periods with the increase in nanohole concentration. This way, the decrease in LIPSS periods could be attributed to the reinforced dipole–dipole coupling for smaller spacings between nanoholes with a typical saturation value of around $3\lambda/4$.

In order to check the proposed scenario, we performed electromagnetic simulations coupled with the two-temperature ablation model. Numerical results revealed the evolution from a rough surface to well-ordered periodic structures by multipulse ablation feedback. The period drops with increasing number of pulses down to the values that are significantly less than the laser wavelength λ and saturates at $3\lambda/4$ at the center of the ablation crater. Additionally, the surface curvature was found to reduce the final periodicity of ripples at the edges of the ablation crater. Both phenomena were explained by surface wave retardation via coupling with neighboring nanoholes or via propagation along the curved interface. The consideration of SPP alone makes it impossible to explain the diversity of the resulting periods, which means that CWs play a crucial role in the final pattern formation.

The results not only elucidate the missing points regarding LIPSS formation and reveal the significance of multipulse electromagnetic feedback in laser-induced nanostructuring but also provide new routes toward optimal light manipulation with sub-wavelength features on metal–dielectric interfaces, development of loss-free metasurfaces, optical guiding, and switching of surface waves.

Acknowledgment: This work was supported by the IMO-TEP project within program “Investissements d’Avenir” operated by ADEME.

References

- [1] Thomas W, Ebbesen HJ, Lezec HF, Ghaemi TT, Wolff PA. Extraordinary optical transmission through sub-wavelength hole arrays. *Nature* 1998;391:667.
- [2] Lalanne P, Hugonin JP. Interaction between optical nano-objects at metallo-dielectric interfaces. *Nat Phys* 2006;2:551.
- [3] Liu H, Lalanne P. Microscopic theory of the extraordinary optical transmission. *Nature* 2008;452:728.

- [4] van Beijnum F, Rétif C, Smiet CB, Liu H, Lalanne P, van Exter MP. Quasi-cylindrical wave contribution in experiments on extraordinary optical transmission. *Nature* 2012;492:411.
- [5] Sobnack MB, Tan WC, Wanstall NP, Preist TW, Sambles JR. Stationary surface plasmons on a zero-order metal grating. *Phys Rev Lett* 1998;80:5667.
- [6] Barnes WL, Dereux A, Ebbesen TW. Surface plasmon subwavelength optics. *Nature* 2003;424:824.
- [7] Perchec JL, Quemerais P, Barbara A, Lopez-Rios T. Why metallic surfaces with grooves a few nanometers deep and wide may strongly absorb visible light. *Phys Rev Lett* 2008;100:066408.
- [8] Zhao LL, Kelly KL, Schatz GC. The extinction spectra of silver nanoparticle arrays: influence of array structure on plasmon resonance wavelength and width. *J Phys Chem B* 2003;107:7343–50.
- [9] Prikulis J, Hanarp P, Olofsson L, Sutherland D, Käll M. Optical spectroscopy of nanometric holes in thin gold films. *Nano Lett* 2004;4:1003–7.
- [10] Jain PK, Huang W, El-Sayed MA. On the universal scaling behavior of the distance decay of plasmon coupling in metal nanoparticle pairs: a plasmon ruler equation. *Nano Lett* 2007;7:2080–8.
- [11] Jenkins JA, Zhou Y, Thota S, et al. Blue-shifted narrow localized surface plasmon resonance from dipole coupling in gold nanoparticle random arrays. *J Phys Chem C* 2014;118:26276–83.
- [12] Stockman MI, Faleev SV, Bergman DJ. Localization versus delocalization of surface plasmons in nanosystems: can one state have both characteristics? *Phys Rev Lett* 2001;87:167401.
- [13] Sánchez-Gil JA. Localized surface-plasmon polaritons in disordered nanostructured metal surfaces: shape versus anderson-localized resonances. *Phys Rev B* 2003;68:113410.
- [14] Huang M, Zhao F, Cheng Y, Xu N, Xu Z. Origin of laser-induced near-subwavelength ripples: interference between surface plasmons and incident laser. *ACS Nano* 2009;3:4062–70.
- [15] Garrelie F, Colombier J-P, Pigeon F, et al. Evidence of surface plasmon resonance in ultrafast laser-induced ripples. *Opt Express* 2011;19:9035–43.
- [16] Bonse J, Höhm S, Kirner SV, Rosenfeld A, Krüger J. Laser-induced periodic surface structures - a scientific evergreen. *IEEE J Sel Top Quantum Electron* 2017;23:109–23.
- [17] Sedao X, Saleh AA, Rudenko A, et al. Self-arranged periodic nanovoids by ultrafast laser-induced near-field enhancement. *ACS Photonics* 2018;5:1418–26.
- [18] Nikitin AY, Garca-Vidal FJ, Martn-Moreno L. Surface electromagnetic field radiated by a subwavelength hole in a metal film. *Phys Rev Lett* 2010;105:073902.
- [19] Zayats AV, Smolyaninov II, Maradudin AA. Nano-optics of surface plasmon polaritons. *Phys Rep* 2005;408:131–314.
- [20] Lalanne P, Hugonin J-P, Liu HT, Wang B. A microscopic view of the electromagnetic properties of sub- λ metallic surfaces. *Surf Sci Rep* 2009;64:453–69.
- [21] Nikitin AY, Rodrigo SG, Garca-Vidal FJ, Martn-Moreno L. In the diffraction shadow: Norton waves versus surface plasmon polaritons in the optical region. *New J Phys* 2009;11:123020.
- [22] Yang XY, Liu HT, Lalanne P. Cross conversion between surface plasmon polaritons and quasicylindrical waves. *Phys Rev Lett* 2009;102:153903.
- [23] van Beijnum F, Sirre J, Rétif C, van Exter MP. Speckle correlation functions applied to surface plasmons. *Phys Rev B* 2012;85:035437.
- [24] Sipe JE, Young JF, Preston JS, van Driel HM. Laser-induced periodic surface structure. I. theory. *Phys Rev B* 1983;27:1141.
- [25] Bonse J, Krüger J, Höhm S, Rosenfeld A. Femtosecond laser-induced periodic surface structures. *J Laser Appl* 2012;24:042006.
- [26] Wang L, Chen Q-D, Cao X-W, et al. Plasmonic nano-printing: large-area nanoscale energy deposition for efficient surface texturing. *Light Sci Appl* 2017;6:e17112.
- [27] Rudenko A, Colombier J-P, Höhm S, et al. Spontaneous periodic ordering on the surface and in the bulk of dielectrics irradiated by ultrafast laser: a shared electromagnetic origin. *Sci Rep* 2017;7:12306.
- [28] Skolski JZP, Römer GRBE, Obona JV, Huis in't Veld AJ. Modeling laser-induced periodic surface structures: finite-difference time-domain feedback simulations. *J Appl Phys* 2014;115:103102.
- [29] Déziel J-L, Dumont J, Gagnon D, Dubé LJ, Messaddeq SH, Messaddeq Y. Toward the formation of crossed laser-induced periodic surface structures. *J Opt* 2015;17:075405.
- [30] Alekseevich IA, Kudryashov SI, Makarov SV, et al. Nonlinear evolution of aluminum surface relief under multiple femtosecond laser irradiation. *JETP Lett* 2015;101:350–7.
- [31] Tsibidis GD, Mimidis A, Skoulas E, et al. Modelling periodic structure formation on 100cr6 steel after irradiation with femtosecond-pulsed laser beams. *Appl Phys A* 2018;124:27.
- [32] Sipe JE, van Driel HM, Young JF. Surface electrostatics: radiation fields, surface polaritons, and radiation remnants. *Can J Phys* 1985;63:104–13.
- [33] Zhang H, Colombier J-P, Li C, Faure N, Cheng G, Stoian R. Coherence in ultrafast laser-induced periodic surface structures. *Phys Rev B* 2015;92:174109.
- [34] Razi S, Varlamova O, Reif J, et al. Birth of periodic micro/nano structures on 316l stainless steel surface following femtosecond laser irradiation; single and multi scanning study. *Opt Laser Technol* 2018;104:8–16.
- [35] Rudenko A, Maclair C, Garrelie F, Stoian R, Colombier J-P. Light absorption by surface nanoholes and nanobumps. *Appl Surf Sci* 2019;470:228.
- [36] Weiner J. Phase shifts and interference in surface plasmon polariton waves. *Opt Express* 2008;16:950–6.
- [37] Inogamov NA, Zhakhovskii VV, Ashitkov SI, et al. Nanospallation induced by an ultrashort laser pulse. *J Exp Theor Phys* 2008;107:1.
- [38] Okamuro K, Hashida M, Miyasaka Y, Ikuta Y, Tokita S, Sakabe S. Laser fluence dependence of periodic grating structures formed on metal surfaces under femtosecond laser pulse irradiation. *Phys Rev B* 2010;82:165417.
- [39] Bévilion E, Stoian R, Colombier J-P. Nonequilibrium optical properties of transition metals upon ultrafast electron heating. *J Phys Condens Matter* 2018;30:385401.
- [40] Abou-Saleh A, Karim ET, Maurice C, et al. Spallation-induced roughness promoting high spatial frequency nanostructure formation on cr. *Appl Phys A* 2018;124:308.

Supplementary Material: The online version of this article offers supplementary material (<https://doi.org/10.1515/nanoph-2018-0206>).